NREL
NATIONAL RENEWABLE ENERGY LABORATORY

Modeling and Control System Design for an Integrated Solar Generation and Energy Storage System with a Ride-Through Capability

Preprint

X. Wang and M. Yue
Brookhaven National Laboratory

E. Muljadi
National Renewable Energy Laboratory

To be presented at the IEEE Energy Conversion Conference and Exposition
Raleigh, North Carolina
September 15–20, 2012

NREL is a national laboratory of the U.S. Department of Energy, Office of Energy Efficiency & Renewable Energy, operated by the Alliance for Sustainable Energy, LLC.

Conference Paper
NREL/CP-5500-55726
September 2012

Contract No. DE-AC36-08GO28308

Available electronically at http://www.osti.gov/bridge

Available for a processing fee to U.S. Department of Energy
and its contractors, in paper, from:

U.S. Department of Energy
Office of Scientific and Technical Information
P.O. Box 62
Oak Ridge, TN 37831-0062
phone: 865.576.8401
fax: 865.576.5728
email: mailto:reports@adonis.osti.gov

Available for sale to the public, in paper, from:

U.S. Department of Commerce
National Technical Information Service
5285 Port Royal Road
Springfield, VA 22161
phone: 800.553.6847
fax: 703.605.6900
email: orders@ntis.fedworld.gov
online ordering: http://www.ntis.gov/help/ordermethods.aspx

Cover Photos: (left to right) PIX 16416, PIX 17423, PIX 16560, PIX 17613, PIX 17436, PIX 17721

Printed on paper containing at least 50% wastepaper, including 10% post consumer waste.

Modeling and Control System Design for an Integrated Solar Generation and Energy Storage System with a Ride-Through Capability

Xiaoyu Wang and Meng Yue
Department of Sustainable Energy Technologies
Brookhaven National Laboratory
Upton, NY 11973, USA
xywang@bnl.gov, yuemeng@bnl.gov

Eduard Muljadi

National Renewable Energy Laboratory
Golden, CO 80401 USA
Eduard_muljadi@nrel.gov

***Abstract*—This paper presents a generic approach for PV panel modeling. Data for this modeling can be easily obtained from manufacturer datasheet, which provides a convenient way for the researchers and engineers to investigate the PV integration issues. A two-stage power conversion system (PCS) is adopted in this paper for the PV generation system and a Battery Energy Storage System (BESS) can be connected to the dc-link through a bi-directional dc/dc converter. In this way, the BESS can provide some ancillary services which may be required in the high penetration PV generation scenario. In this paper, the fault ride-through (FRT) capability is specifically focused. The integrated BESS and PV generation system together with the associated control systems is modeled in PSCAD and Matlab platforms and the effectiveness of the controller is validated by the simulation results.**

I. INTRODUCTION

With ever increasing concerns on energy security and environmental issues, utilization of renewable energy generation has gained rapid development and global acceptance over the past few decades. Among those sources, photovoltaic (PV) generation appears to be one of the most promising technologies due to the abundance of solar insolation in various regions, the absence of moving parts in the generation system, it requires no transmission lines (e.g. roof top PV installations), and low operation and maintenance costs. In 2010, the PV installation capacity across the world increases to 14.2 GW, which represents a doubling of the amount in year 2009. The same trend was observed in the US, and the accumulated installed capacity across the nation reached 2.5 GW by the end of 2010. This trend is expected to continue throughout the next decade, driven especially by both the decline of PV panel cost and the favorable policy initiatives from federal and local level governments [1]. As large amounts of PV generation are adopted, the PV systems are moving from small scale generation (i.e. roof top system connected to the distribution system) to the large scale generation (i.e. centralized PV plant connected to the transmission) [2].

The code requirements for grid-connected PV generation have undergone a continuous evolution in recent years. Among these requirements, grid support functions are prohibited in present interconnection standards such as IEEE 1547 or UL 1741, which requires that the renewable generation be disconnected from the mains system when abnormal conditions occur on the grid side. The voltage at the point of interconnection (POI) is not regulated by the renewable energy power plant [3, 4]. However, with increasing penetration levels of renewable generation, the solar POIs are changing from the distribution system to sub-transmission or transmission systems, and the standards have been updated (e.g. FERC Order 661 and 661A) to require the grid-connected renewable energy generation provide ancillary capabilities during fault and post-fault durations [5, 6]. These ancillary capabilities include the fault ride-through capability, reactive power control capability to regulate voltage or power factor, and the SCADA systems. These ancillary services can potentially prevent cascading event that may lead to blackout, improve recovery process from the fault events, and enhance the system stability. To provide these ancillary services, the PV plants must be able to stay online as long as possible and ride through the fault events that originate in the grid until the fault event is cleared or the relay protection tripped the PV plant. The FRT requirements proposed in FERC Order 661A is shown in Fig. 1.

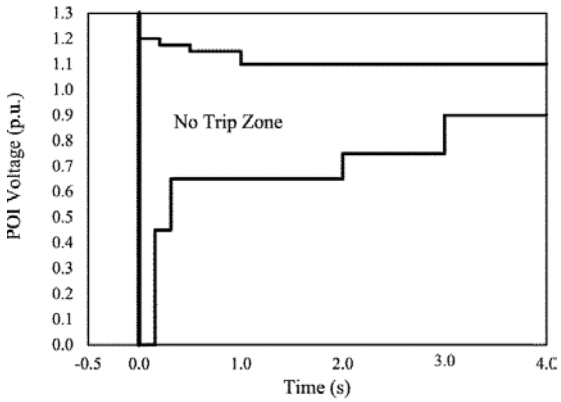

Figure 1. Example FRT curve (FERC Order 661A).

The FRT capability of solar energy systems has been investigated in other work [5-7]. However, some manufacturers implement FRT capability by decreasing the output power of the PV generation while maximizing the reactive power (to limit the IGBT current from exceeding its designed rated value) to support the voltage drop during the fault. This is implemented by shifting the PV panel operational voltage away from its maximum power point (MPP) generation. This implementation sacrifices power generation over the fault durations, and degrades the efficiency of the PV plants. This is particularly important for large grid-connected solar plants that generate hundreds of megawatts, where the reduction of power generation over the transients will become so significant that it cannot be neglected, as indicated in [8]. One possible approach to address this issue is to use the solar plant output to charge an energy storage system (ESS) during the fault ride-through period without shedding the solar PV generation while the contribution to the fault current is still reduced or eliminated. It is assumed that the ESS is installed at the dc bus of the power inverter as shown in Fig. 2.

In the present interconnection standards, the power inverters are disconnected immediately from the grid when voltage dips at the POI due to, for example, faults in the grid [3, 4]. The purpose of this is to prevent fault current contribution from the solar plant and is beneficial to the system operation. As the size of the solar PV plant increases above 10MW, the requirement does not follow IEEE1547 and it is considered to be a conventional power plant. If a curtailment of solar generation is not preferred and the solar plant still operates at MPP condition, the ride-through of PCS inverters contributes to the fault current and thus will deteriorate the voltage condition at the POI [3]. With deployment of the ESS and the proper control, the power generated by the solar plant can be delivered to the grid and/or ESS as needed. The discharging ESS acts as a generator and the ESS being charged acts as an active load. The fault current contribution from the solar plant can be constrained by the current controllability of the solar power inverter having the current control capability.

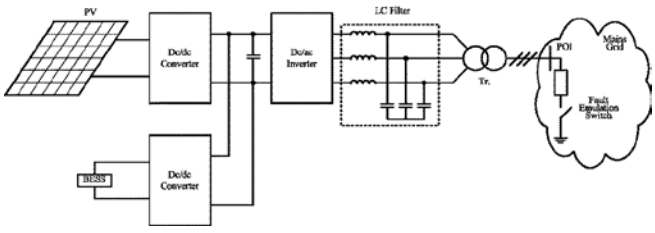

Figure 2. Overall system diagram of PV/BESS.

Another benefit of incorporating an ESS into a solar PV plant is that by reducing the real power flowing into the grid, the grid side PCS inverter capacity can be fully utilized for the reactive power injection to support voltage recovery at the POI during and after fault event.

A third advantage of storage is to reduce the output fluctuations caused by the variation of solar irradiance during the passing clouds. However, this point will not be focused on in this paper.

Though ESS connection port had been proposed and provided for the AC-link technology based PCS in [8], no details of the control schemes for the converter were provided. The ESS system had not been incorporated in [8]. In this paper, a PCS incorporating ESS and solar generation will be investigated in detail. Especially controllers will be designed with the FRT and voltage support capabilities for the PCS and their effectiveness will be demonstrated via simulations. The proposed system is modeled in combination of PSCAD and Matlab platforms.

The contents of this paper are arranged as follows: background review is provided in Section I, followed by the description of system in Section II. Modeling of components of solar array and battery energy storage systems and the associated control systems are presented in Section III. Simulation results are presented in Section IV. Concluding remarks are given in Section V.

II. System Description

The PCS for solar power plants (and other types of grid-connected renewable energy sources such as wind and fuel cells etc.) may have different architectures, e.g., a single-stage (a grid-connected inverter only) or a two-stage (a dc/dc converter and a grid-connected inverter) PCS [9, 10]. The latter structure, as shown in Fig. 2 is more popular and selected to interface the PV power plant with the transmission network due to an extra degree of freedom it may provide. In this topology, the function of the PV-connected dc/dc converter is to track the MPP of the solar plant through regulating the PV modules' output voltage. The dc/dc converter steps up the solar dc output voltage to a level higher than the voltage value of the POI such that a step-up transformer may not be needed for a voltage-source inverter to inject power into the grid. This approach has been proposed in the transformer-less PV inverter studies by using the emerging power electronic devices with high power capacity [11-13]. This approach is not adopted in this paper, and a step-up transformer is utilized, as shown in Fig. 2. The grid interfaced inverter converts the dc to ac and controls the real and reactive powers flowing into the grid instantaneously and independently.

In the PCS system described above, a BESS is connected to the dc-link within a solar power plant. The charging and discharging processes are fulfilled by regulating the current through adjusting the associated dc/dc converter of the BESS. This can compensate for the output power intermittency from the PV plant under normal conditions, i.e., the variability of solar irradiance due to passing clouds. Other grid support function such as frequency regulation can also be provided by the PV plant with assistance of BESS. In these cases, BESS is able to dispatch power to, as well as receive power from the dc-link to charge itself while the solar plant is always operating at MPP to achieve highest available efficiency. Therefore, a bi-directional dc/dc converter is implemented for the BESS, as shown in Fig. 2.

These intermittency smoothing and frequency regulation functions have been investigated by the authors and will be presented in another paper. The focus of this paper is on the function of the BESS to store the solar power during the fault condition and thus enables the grid-connected inverter to provide voltage support and ride through a fault event.

III. Modeling of Solar Power Generation and Battery Energy Storage System

A. Solar Array

In this section, a generic solar generation model is developed based on manufacturers' data to include the solar irradiance and temperature. In general, a solar module is manufactured by connecting a number of solar cells in series. A solar array consists of a number of solar modules connected in series and parallel. Therefore, the basic step in modeling a solar array or power plant is to analyze a single solar cell, which can be modeled with various complexities. In this study, a solar cell is essentially represented by an equivalent electrical circuit consisting of a photon current source (I_{Ph}), a diode and a shunt resistance in parallel (R_P and can be generally neglected) and a series resistance R_S, as shown in Fig. 3, where I_d is the current of the diode, and I_{PV} and V_{PV} indicate the solar cell terminal output current and voltage, respectively. The description of this circuit can be found in many references, e.g., [14], and a brief summary will be given in this paper for the purpose of illustration only.

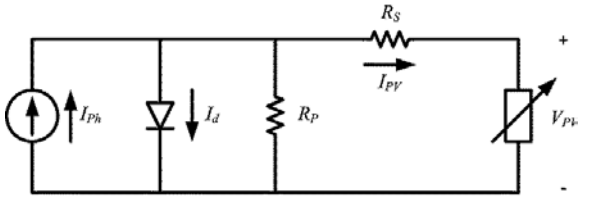

Figure 3. An equivalent electrical circuit of a solar cell.

In Fig. 3, for a given cell temperature (T) and irradiance (G), the output current of the solar sell can be expressed in,

$$I_{PV} = I_{Ph} - I_d - \frac{V_{PV} + I \times R_S}{R_P} \tag{1}$$

where I_{Ph} , I_d and R_S can be calculated by,

$$I_{Ph}|_{T,G} = \frac{G}{G_{ref}} I_{SC,ref}[1 + \alpha(T - T_{ref})] \tag{2}$$

$$I_d|_{T,G} = \frac{I_{SC,ref}}{e^{\frac{qV_{OC,ref}}{nkT_{ref}}} - 1} \times \left(\frac{T}{T_{ref}}\right)^3 e^{\frac{qE_g}{nk}\left(\frac{1}{T_{ref}} - \frac{1}{T}\right)} \times \left(e^{q\frac{V_{PV} + I_{PV} \times R_S}{nkT}} - 1\right) \tag{3}$$

$$R_S = \frac{nkT_{ref}}{qI_{m,ref}} \ln\left[e^{\frac{qV_{OC,ref}}{nkT_{ref}}} - \frac{I_m}{I_{SC,ref}}\left(e^{\frac{qV_{OC,ref}}{nkT_{ref}}} - 1\right)\right] - \frac{V_{m,ref}}{I_{m,ref}} \tag{4}$$

The constants and/or quantities in (2)-(4) are given as follows. G_{ref} = 1000 W/m^2, T_{ref} = 298 K , $V_{oc,ref}$, $I_{sc,ref}$, $V_{m,ref}$ and $I_{m,ref}$ are the irradiance, panel temperature, open circuit voltage, short circuit current, panel MPP voltage and current at MPP under standard condition. α is the temperature coefficient of the short circuit current. $q = 1.602e^{-19}$ C is the Coulomb constant, $k = 1.38e^{-23}$ J/K the Boltzmann constant. n is the diode ideality factor which is between 1-2. E_g is band-energy gap (eV) and can be quantified as $E_g = 1.16 - 0.000702\frac{T^2}{T - 1108}$. All the above listed quantities can be found from examining the manufacturer datasheet and the published I-V curves of the PV module.

In this paper, a PV module is implemented in PSCAD by connecting a controlled current source to a diode in parallel and then to a series resistor, R_S. Since the effect of parallel resistor, R_P is negligible, one can set a very high value in the equivalent circuit implementation.

After the PV module is built, it can be scaled up to a PV array model containing N_s panels connected in series and N_p strings in parallel. The numbers of N_s and N_p can be specified based on the specifications of the string voltage rating and the capacity of the PV farm respectively, as to be illustrated in the simulation part.

B. Battery Energy Storage System

Several equivalent battery circuit models have been reported in the literature. The models are applicable to study the battery behavior over short or long-term intervals during its charge/discharge process [15, 16]. Some physics-based models have been developed to study the internal chemical dynamics of lead-acid batteries. However, these models are generally not suitable for electrical system design exercises because chemical time constant is much higher than electrical time constant. Though the capacitor/resistor branches based models, like the fourth order model [17] can describe the nonlinear phenomena within the battery, they become dramatically complex in the modeling process. In this study, the voltage source-resistor model, as shown in Fig. 4 is selected to avoid detailed calculations of internal electrochemical processes. However, the internal resistors are differently specified based on the charge and discharge cases, as described in the next contents.

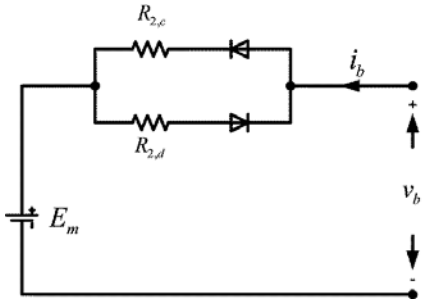

Figure 4. Equivalent circuit of lead acid battery.

In this model, E_m denotes the battery internal e.m.f, which is the open circuit voltage at no load condition. The internal resistance, R_2 has two components, $R_{2,c}$ and $R_{2,d}$, which contribute to the power loss inside the battery units under charge and discharge conditions respectively. The charge/discharge current is depicted by i_b and the terminal voltage v_b. In Fig. 4, positive values of i_b denote charging and negative values for discharging currents. Note in this model that the e.m.f, E_m and the electrical parameters, $R_{2,c}$ and $R_{2,d}$ are all functions of the state of charge (*SOC*) of the battery and its operation temperature, T_{emp}. Therefore, E_m, $R_{2,c}$, and $R_{2,d}$ are indexed by *SOC* and T_{emp} through a 2-dimention look-up table in this study.

The *SOC* is obtained by the following equation,

$$SOC = 1 - \frac{Used \quad Ah \quad Capacity}{Max \quad Ah \quad Capacity} \tag{5}$$

where the used Ah capacity is calculated by,

$$\text{Used Capacity} = \begin{cases} Q_e(t_0) + \int_0^t \eta_{coulomb} i_b(t)\,dt, & \text{for } i_b(t) \geq 0 \text{ chg.} \\ Q_e(t_0) + \int_0^t i_b(t)\,dt, & \text{for } i_b(t) < 0 \text{ dischg.} \end{cases} \tag{6}$$

where $Q_e(t_0)$ is the initial capacity at the starting instant of charging/discharging and $\eta_{coulomb}$ is the coulombic efficiency.

Another consideration in this model is that the internal resistance, R_2 during the charge and discharge processes has different values. Based on the current direction, the internal resistance can be selected by,

$$R_2 = \begin{cases} R_{2,c}(SOC, T_{emp}) & \text{for } i_b \geq 0 \\ R_{2,d}(SOC, T_{emp}) & \text{for } i_b < 0 \end{cases} \tag{7}$$

Therefore, the battery terminal voltage is derived by,

$$v_b(SOC, T_{emp}) = E_m(SOC, T_{emp}) + i_b R_2(SOC, T_{emp}) \tag{8}$$

In this paper, the internal E_m and R_2 are determined by the *SOC* and T_{emp} from two two-dimension lookup tables respectively, which are obtained from the experimental test of Hawker Genesis 12V26Ah10EP sealed valve-regulated lead-acid battery. The open circuit voltage of each unit is set from 11.7 to 12.89 V corresponding to *SOC* from 0 to 1.

Based on the battery cell described above, one can easily scale it up to a BESS consisting of a number of cells connected in series and parallel depending on the capacity specified.

C. Controller design for the PV dc/dc converter

A unidirectional-boost-converter was selected to convert the power captured by the PV panel at lower voltage level to a higher voltage level, in such a way that the low voltage PV system can be adopted and cost of the conversion system can be reduced (refer to Figure 5).

The PV model represents the model built in Section III.A, with the voltage and current outputs denoted by v_{PV} and i_{PV}. The capacitor C_{PV} is used to filter out the high frequency harmonics which may cause negative influence on the operation of PV panel. The current input to the boost converter is i_{LPV} and the output voltage is v_{dc} which is also the dc-link voltage across *C*.

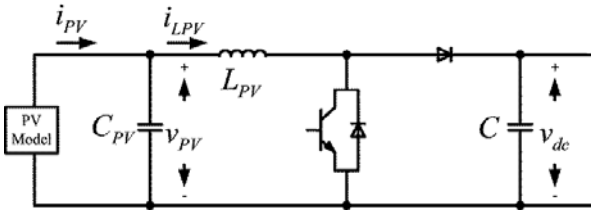

Figure 5. PV system connected with boost converter.

In steady state, the following relationship holds between the output and input voltages of the boost converter,

$$\frac{V_{dc}}{V_{PV}} = \frac{1}{1-D} \qquad 0 \leq D \leq 1 \tag{9}$$

where D is the duty ratio of the dc/dc converter. (9) indicates that, if the dc-link voltage is maintained constant, which is controlled by the BESS converter in this study, the PV output voltage can be regulated through adjusting the duty ratio to achieve MPP tracking (MPPT) of the PV array.

The control system for the boost converter is shown in Fig. 6.

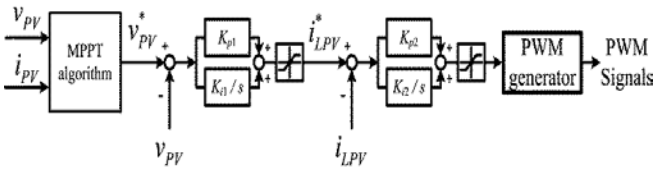

Figure 6. Control system for the PV boost converter.

In this control system, the outer voltage loop regulates the PV output voltage to track the MPP by using a PI compensator and the inner current loop regulates the inductor current to reduce the high frequency harmonics occurring in the inductor.

It is noted that the MPPT algorithm used in this paper is a modified algorithm which can improve the conversion efficiency of the PV generation system. This algorithm is implemented in Matlab scripts and interfaced to PSCAD using the language provided by EMTDC. Interested readers can find more detailed descriptions of this algorithm in [18].

D. Controller design for the BESS dc/dc converter

In the integration of BESS with PV system, the BESS can be charged or discharged to absorb from or release power to the dc-link. Therefore the power flow can flow in and out of the BESS and a bi-directional dc/dc converter is required for the BESS. There exist two categories of bi-directional dc/dc converter topologies proposed in the

literature, isolated and no-isolated. Due to the existence of the high frequency transformers which increase the design complexity of the former category, a simple but effective non-isolated bi-directional dc/dc converter is adopted in this paper, as shown in Fig. 7.

In Fig. 7, the BESS model developed in Section III.B is implemented. Note, the bi-directional dc/dc converter is based on the boost topology, which means the BESS voltage v_b is always lower than that of dc-link. To fulfill the bi-directional power flow conversion, the two switches within the dc/dc converter, S_1 and S_2 need to be coordinated as discussed below.

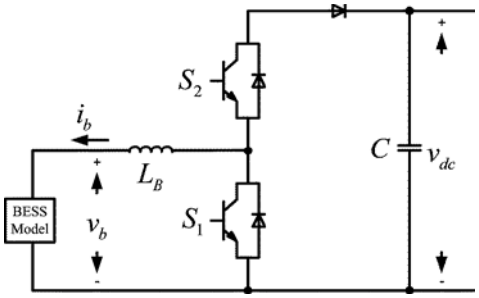

Figure 7. BESS connected to dc-link through bi-directional converter.

Under BESS discharging situation, where $i_b < 0$, the dc/dc converter functions as a boost converter, looking from the BESS side. Therefore, S_2 is de-activated while only S_1 is working. Note that the diodes are not controllable switches. In steady state, the relationship depicted by (9) still holds for the two voltages v_{dc} and v_b. When the BESS is in the charging process, S_1 is de-activated and S_2 is working such that the power flows from dc-link to BESS. Under which condition, the dc/dc converter is working as a buck converter and in steady state the relationship between V_b and V_{dc} is depicted by the following equation,

$$\frac{V_b}{V_{dc}} = D \qquad 0 \le \mathrm{D} \le 1 \tag{10}$$

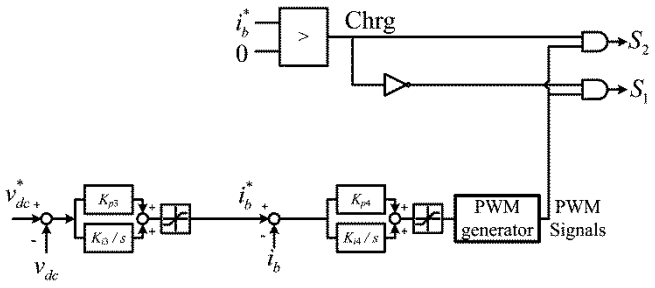

Figure 8. Control system for the BESS bi-directional converter.

To implement the above operation scheme of the dc/dc converter, its controller system design is shown in Fig. 8. The inner current loop regulates the BESS current to track the given command i_b^*. The outer voltage loop regulates the dc-link voltage to the reference value and generates for the inner loop a reference signal, i_b^*. To improve the dynamic performance of the inner loop, the following scheme is adopted depending on the judgment of i_b^* direction, flag Chrg. The de-activation/working status of S_1 and S_2 will be determined by value of Chrg, instead of comparison of dc-link voltage against its reference value. This approach can avoid the frequent transitions of the power flow directions and the topology switching back and forth between the buck and the boost topologies. This may contribute to the better dynamic performance of the controller especially during the transition from charging status to discharging or vice versa.

E. Controller Design for FRT Capability of the Grid-Integrated Solar Generation

The topologic configuration with the associated control scheme of the grid-tie inverter is shown in Fig. 9.

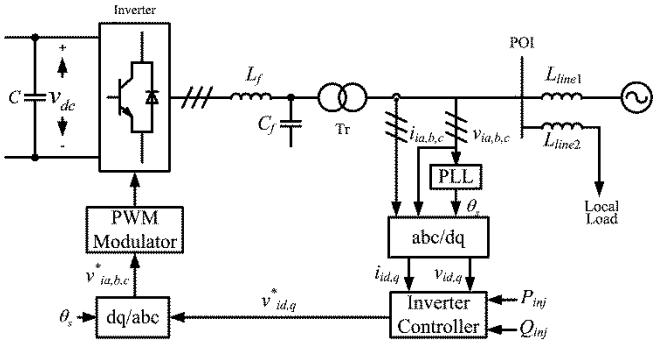

Figure 9. Inverter topology of the grid-tie inverter.

With the application of digital controllers, the synchronous reference frame control or *d-q* control has become very popular for controlling the grid-connected inverters. The basic concept of the *d-q* control is to perform a reference frame transformation from the stationary coordinate system (*a-b-c* coordinate) to a reference frame that is synchronously rotating with the *a-b-c* frame, i.e., a *d-q* transformation (see, e.g., [19]). After the transformation, the real and reactive powers of the inverter can be controlled separately by regulating the *d*-axis and the *q*-axis current injections into the grid, respectively, as shown in (11),

$$\begin{cases} P_{inj} = 3/2 I_{id} * V_{id} \\ Q_{inj} = -3/2 I_{iq} * V_{id} \end{cases} \tag{11}$$

Based on this decoupled *d-q* reference frame, the control system for the grid-connected inverter can be designed consisting of two cascaded loops, as shown in Fig. 10. The inner loop regulates the *d*- and *q*-axis currents while the outer loop regulates the real and reactive power injections at POI. The reactive power reference is generated by the voltage controller which is used to regulate the POI voltage to its nominal value, even over the fault time duration. The real power reference under the normal condition can be selected as a constant value to mitigate the negative influence caused by the intermittent PV generation on the grid. The mismatched power between the PV generation and the desired amount of real power injection into the grid is provided by the BESS whose control system regulates the dc-link voltage to be constant.

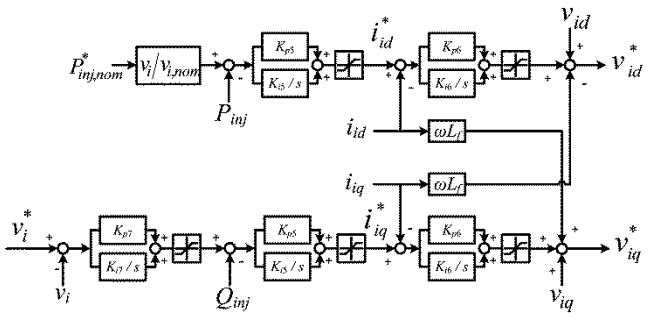

Figure 10. Control system for the grid-tied inverter.

When a fault occurs in the grid and causes voltage at POI to divert from its nominal value, $v_{i,nom}$, to v_i, which is within the envelop of the FRT curve (no trip zone – refer to Fig. 1). Note that if the POI voltage is outside the boundary of the FRT curve, the PV system has to be tripped off and the power injection into the grid becomes zero. Otherwise the real power that can be transmitted to the grid decreases proportionally by a factor $v_i/v_{i,nom}$, when the inverter current is at its rated value. Therefore, the *d*-axis current will drop accordingly and the *q*-axis current can be increased and more reactive power is injected to the grid to provide voltage support at POI. Meanwhile, with the presence of the BESS the system is able to absorb the surplus power that cannot be transfer out to the grid during faults, the PV system can still be operated at MPP and the dc-link voltage can be maintained.

Such controlled BESS can provide FRT capability for the PV system as well improves the efficiency of the PV generation system, since the stored energy can be appropriately released to the grid after fault events.

IV. Simulation Results

The PV-BESS generation system shown in Fig. 2 with the associated control systems as described in Section III has been modeled in the PSCAD/EMTDC platform. Some of the system specifications are described as below.

In this simulated system, a 1 MW PV array consisting of series and parallel connected PV panels from BP Solar, BP 3225T [20] was modeled following the procedure in Section III.A. From the data sheet of BP 3225T, one can find that the rating voltage of the panel at standard condition is 29.1 V. With the rated input voltage level for the dc/dc converter is selected to be 600V, the series connected number panel is 20. The power rating for each string is 4.5 kW and the parallel connected string number is 222 for a 1 MW output.

For illustration, the BESS capacity was also specified to be 1 MW. From the specifications of Hawker Genesis 12V26Ah10EP, the rating value of the battery cell is 12 V. At terminal voltage of 600V, the BESS needs 50 cells connected in series for each string. The capacity of the battery cell is C_5 = 0.05 Ah (or 0.05/5 Ah per-cell). Therefore, the parallel connected string number in the BESS can be computed as 1M/(50*12*0.05/5*3600) = 46 with an energy capacity of 1MW-seconds.

The dc-link voltage is kept at 1.2 kV at normal condition, which is maintained by the BESS dc/dc converter. The grid-tie inverter converts the dc-link voltage to 0.575 kV ac (line to line rms value) and then step up to 10 kV by a transformer which is connected to the mains grid through a 7 km overhead line, Line1 as indicated in Fig. 9. The mains grid is represented by a Thevenin equivalent circuit. A 10 MW resistive local load is also included in the grid and is connected to the POI through another 7 km overhead line, Line2.

The PI constants selected for the controllers in the system are listed in Table I.

TABLE I. PI CONSTANTS USED IN THE SIMULATION.

K_{p1}	K_{i1}	K_{p2}	K_{i2}	K_{p3}	K_{i3}	K_{p4}	K_{i4}
4e-6	5e-5	4e-6	5e-5	1	0.1	4e-6	5e-6
K_{p5}	K_{i5}	K_{p6}	K_{i6}	K_{p7}	K_{i7}		
0.2	0.01	10	0.1	10	0.4		

To validate the effectiveness of the control system designed in this paper, a three phase to ground fault is simulated on Line2 at t = 10 s and is cleared at t = 11 s. Note that the actions of the protection devices are not considered in this study to investigate the function of the designed control system. Some of simulation results are shown in this part.

In the first scenario, a simulation is done to investigate the system performance for the fault event while no FRT capability is equipped with the PV inverter, which means the PV generation is tripped immediately after the fault incident occurs. Note that in this case the BESS is connected to the dc-link throughout the fault duration. The simulation results are shown in Figs. 11 and 12 respectively.

Observation of the top trajectory of Fig. 11 shows that the POI voltage drops from 1.0 to 0.7 p.u. of its original value during the fault event. The real and reactive power injections to the grid are shown in the bottom two trajectories of Fig. 11 respectively, which decrease to zero due to the disconnection of the PV system from the grid. This disconnection causes the recovery process after the fault event lasts longer than that in the case with FRT capability, as will be shown in Fig. 13, which is more favorable from the system operation point of view.

The performance of the BESS during this event is shown in Fig. 12, from which one can find that the variations of the BESS voltage, current and power over the fault duration are more dramatical compared with the case shown in Fig. 15. Especially, the dc-link voltage in this case increases up to 2 p.u. of its nominal value, which is so high that the power electronic devices may be damaged (additional cost due to

repairs) if protection measures are not taken into consideration.

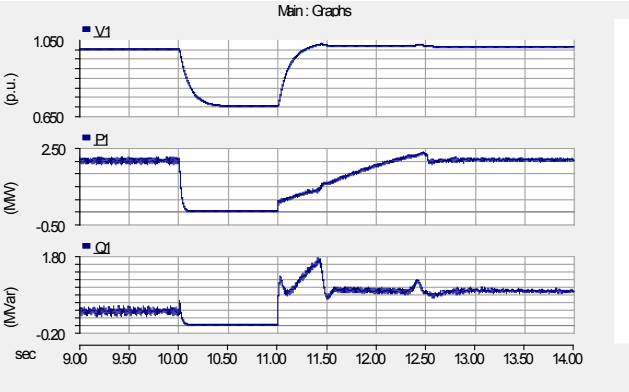

Figure 11. Simulation results of the POI voltage magnitude and the real and reactive power injections at POI (without FRT).

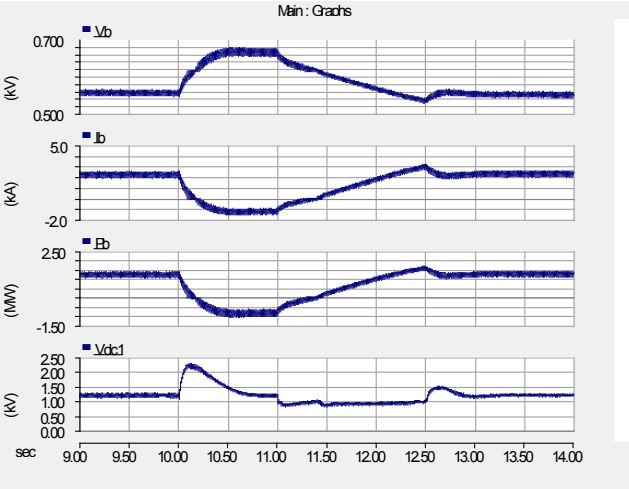

Figure 12. Simulation results of the BESS (without FRT).

For comparison, another simulation is done to investigate the system performance for the same fault event while FRT capability is equipped with the PV inverter, which means the PV generation is always connected throughout the fault incident. Results are shown in Figs. 13-15.

As can be found in Fig. 13, the POI voltage magnitude drops to 0.8 p.u., which is higher than that given in Fig. 11. This is because the PV generation can provide voltage support in this case. The real power reference decreases accordingly and the actual real power injected to the grid can perfectly track its reference value, decreasing from 2 MW to 1.6 MW. This ensures that the current limit of the IGBTs in the converter is not violated. In the meantime, the reactive power injected to the grid increases due to the deviation of POI voltage from its nominal value, which contributes to the voltage support at POI. It is noted that due to the strong connection between the POI and the mains grid in this study, the POI voltage cannot be easily supported up to its original value. However, the effectiveness of the voltage support provided by the PV system during the fault can be observed in Fig. 13, compared the results given in the top trajectory of Fig. 11.

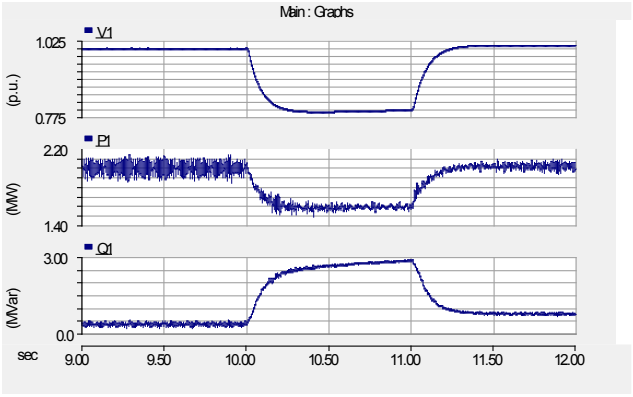

Figure 13. Simulation results of the POI voltage magnitude and the real and reactive power injections at POI (with FRT).

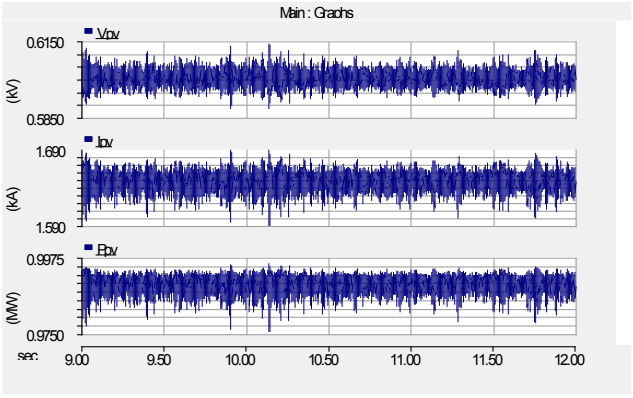

Figure 14. Simulation results of the PV array (with FRT).

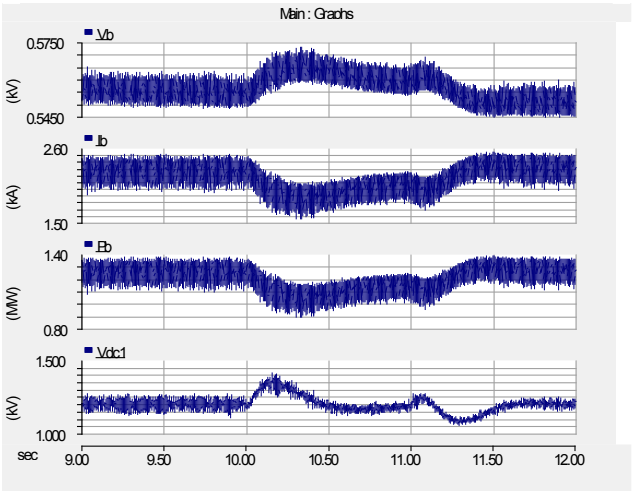

Figure 15. Simulation results of the BESS (with FRT).

Simulation results of the PV array in this case are given in Fig. 14. In this simulation, it is assumed that the irradiance over the simulated period is 1000 W/m^2 and the PV array is controlled to be always operated at MPP. Therefore, the PV array voltage is kept at 600 V through the MPPT algorithm.

The overall output current is 1.66 kV and the power generated by the PV array is 1 MW.

Fig. 15 shows the simulation results of BESS over this time period, from the bottom trajectory one can find that the dc-link voltage is always kept around its reference value, 1.2 kV. Under the normal condition, the BESS terminal voltage is 0.555 kV and discharging current is 2.25 kA. The power generation from the BESS is 1.25 MW. Comparing the power injection result at the normal condition, center trajectory in Fig. 13, one can see that after fault occurs, the real power injected to the grid is reduced from 2MW to 1.6 MW, while the PV array is still operated at MPP, generating 1 MW power (bottom trajectory in Fig. 14) and that the power output of BESS is reduced to 1.1 MW (third trajectory in Figure 15). The top two trajectories show the BESS terminal voltage and current respectively.

V. CONCLUSIONS

A BESS incorporated PV conversion system is studied in this paper. Control systems for the BESS regulation converter and grid interconnected inverter are designed to fulfill the FRT capability. Through the proposed FRT scheme, the BESS stores power generated by the PV plant enabling it to continue operation in MPP condition for the duration of the fault. At the same time, the spare capacity of the grid side inverter can be used to support the system operation by providing additional reactive power injection to the grid, to its maximum current carrying capability of the power switches if needed. In this way, the PV plant can play its role to assist the system in smoothly recovering from disturbances and maintain grid stability during the fault and in the post fault recovery period. Simulations were performed that verified the effectiveness of the proposed control systems.

REFERENCES

[1] "Trends in Photovoltaic Applications," IEA Report IEA-PVPS T1-20:2011, 2011.

[2] S. Achilles, S. Schramm, J. Bebic, G. G. Research, and N. R. E. Laboratory, *Transmission system performance analysis for high-penetration photovoltaics*: National Renewable Energy Laboratory, 2008.

[3] J. Keller and B. Kroposki, "Understanding Fault Characteristics of Inverter-Based Distributed Energy Resources," Technical Report, NREL/TP-550-46698, Jan., 2010.

[4] Z. Ye, R. Walling, L. Garces, R. Zhou, L. Li, and T. Wang, "Study and Development of Anti-Islanding Control for Grid-Connected Inverters," NREL/SR-560-36243, May 2004.

[5] C. H. Benz, W. T. Franke, and F. W. Fuchs, "Low voltage ride through capability of a 5 kW grid-tied solar inverter," in *Power Electronics and Motion Control Conference (EPE/PEMC), 2010 14th International*, 2010, pp. T12-13-T12-20.

[6] E. H. Camm and S. E. Williams, "Solar power plant design and interconnection," in *Power and Energy Society General Meeting, 2011 IEEE*, 2011, pp. 1-3.

[7] A. Marinopoulos, F. Papandrea, M. Reza, S. Norrga, F. Spertino, and R. Napoli, "Grid integration aspects of large solar PV installations: LVRT capability and reactive power/voltage support requirements," in *PowerTech, 2011 IEEE Trondheim*, 2011, pp. 1-8.

[8] E. Limpaecher, G. Deffley, F. Hoffmann, and Z. Wei, "750kW AC-link power converter for renewable generation and energy storage applications," in *Energytech, 2011 IEEE*, 2011, pp. 1-6.

[9] W. Kramer, S. Chakraborty, B. Kroposki, and H. Thomas, "Advanced Power Electronic Interfaces for Distributed Energy Systems, Park 1: Systems and Topologies," Technical Report, NREL/TP-581-42672, March, 2008.

[10] F. Schimpf and L. E. Norum, "Grid Connected Converters for Photovoltaic, State of the Art, Ideas for Improvement of Transfomerless Inverters," Nordic Workshop on Power and Industrial Electronics, June, 2008.

[11] O. Lopez, F. D. Freijedo, A. G. Yepes, P. Fernandez-Comesaa, J. Malvar, R. Teodorescu, and J. Doval-Gandoy, "Eliminating Ground Current in a Transformerless Photovoltaic Application," *Energy Conversion, IEEE Transactions on,* vol. 25, pp. 140-147, 2010.

[12] M. C. Cavalcanti, K. C. de Oliveira, A. M. de Farias, F. A. S. Neves, G. M. S. Azevedo, and F. C. Camboim, "Modulation Techniques to Eliminate Leakage Currents in Transformerless Three-Phase Photovoltaic Systems," *Industrial Electronics, IEEE Transactions on,* vol. 57, pp. 1360-1368, 2010.

[13] H. Xiao, S. Xie, Y. Chen, and R. Huang, "An Optimized Transformerless Photovoltaic Grid-Connected Inverter," *Industrial Electronics, IEEE Transactions on,* vol. 58, pp. 1887-1895, 2011.

[14] S.-K. Kim, J.-H. Jeon, C.-H. Cho, E.-S. Kim, and J.-B. Ahn, "Modeling and simulation of a grid-connected PV generation system for electromagnetic transient analysis," *Solar Energy,* vol. 83, pp. 664-678, 2009.

[15] C. J. Zhan, X. G. Wu, S. Kromlidis, V. K. Ramachandaramurthy, M. Barnes, N. Jenkins, and A. J. Ruddell, "Two electrical models of the lead-acid battery used in a dynamic voltage restorer," *Generation, Transmission and Distribution, IEE Proceedings-,* vol. 150, pp. 175-182, 2003.

[16] M. Ceraolo, "New dynamical models of lead-acid batteries," *Power Systems, IEEE Transactions on,* vol. 15, pp. 1184-1190, 2000.

[17] R. Giglioli, A. Buaonarota, and P. Cerolo, "Charge and discharge fourth order dynamic model of lead battery," presented at the 10th Inernational Electrical Vehicle Symposimu, HK, 1990.

[18] M. Yue, X. Y. Wang, J. Lorafo, and M. Villaran, "IEEE Trans. on Sustainable Energy," Submitted to.

[19] F. Blaabjerg, R. Teodorescu, M. Liserre, and A. V. Timbus, "Overview of control and grid synchronization for distributed power generation systems," *IEEE Transactions on Industrial Electronics,* vol. 53, pp. 1398-1409, 2006.

[20] *BP 3225T Data Sheet, http://www.fplsolar.org/wp-content/uploads/BP3225T_1-10.pdf*.